Science and Technology of High Pressure, Proceedings of the AIRAPT-17,
edited by M.H. Manghnani, W.J. Nellis and M.F. Nicol, pp. 68-73, University Press, Hyderabad, India, 2000.

Finite-Element Modeling and Ab initio Calculations of Megabar Stresses in the Diamond Anvil Cell

Sébastien Merkel*, Russell J. Hemley, Ho-kwang Mao and David M. Teter†
Geophysical Laboratory and Center for High Pressure Research, Carnegie Institution of Washington, 5251 Broad Branch Rd., N.W., Washington, DC 20015, U.S.A.

Finite-element modeling calculations are conducted to investigate the remarkably large elastic strains in diamond observed in ultrahigh pressure diamond anvil cell experiment. We perform *ab initio* calculations to evaluate the elastic properties of diamond in the multimegabar range and use the £nite-element results to estimate the pressure dependence of shear stress of strong materials used as gasket. We then analyze the in¤uence of geometric properties such central ¤at diameter or bevel angle, and reveal the existence of two distinct deformation mechanisms during the pressure increase. Finally, we investigate the stress conditions in the gasket and the diamond and discuss possible shear-induced mechanical instabilities in diamond.
[£nite-element modeling, ab-initio calculations, large deformations, stress, failure]

1. Introduction

The diamond anvil cell is widely used in the £eld of high pressure research for the generation of extreme static pressure conditions. Diamond's strength, high electrical resistivity, high thermal conductivity and transparency over a wide range of wavelengths allows *in situ* measurements on materials under a variety of pressure and temperature conditions. Beveled diamonds concentrate the stress on the sample allowing the multimegabar range to experiments[1, 2]. Understanding the behavior of the anvil under these conditions is essential for extending the range of feasible laboratory static pressures. Recent x-ray experiments[3] imaged the deformations of the diamond tip under multimegabar pressures. Finite-element modeling[4] then con£rmed that, although often considered to be a rigid body, diamond could sustain signi£cant large elastic deformations near the sample region. In this study, we discuss the material properties that are critical for such calculations. We present results from *ab initio* calculations of the elastic properties of diamond in the multimegabar range and a means to estimate the gasket yield stress. We then extend the previous £nite-element calculations[4, 5, 6, 7] to provide a better understanding of the in¤uence of geometric properties such as the diamond bevel angle and central ¤at diameter.

2. Model

We performed two-dimensional axisymmetric £nite-element calculations using NIKE2D (e.g., Refs. [4, 6, 7]) that includes rezoning capabilities. Because of the very large deformations observed in the gasket, the rezoning plays a very important role by allowing modi£cation of the grid during the calculations. The axial symmetry implies that coordinates and stresses have to be expressed in cylindrical system r, θ and z whose z is parallel to the loading axis, r is the radial distance from the z axis, and θ is perpendicular to r and z. The stress components are independent of the θ coordinate ($\partial\sigma_{ij}/\partial\theta = 0$), and the only stresses considered are σ_{rr}, σ_{zz}, $\sigma_{\theta\theta}$ and σ_{rz} with $\sigma_{r\theta}$ and $\sigma_{\theta z}$ always equal to zero. The symmetry also implies that along the z axis ($r = 0$), $\sigma_{\theta\theta} = \sigma_{rr}$ and $\sigma_{rz} = 0$.

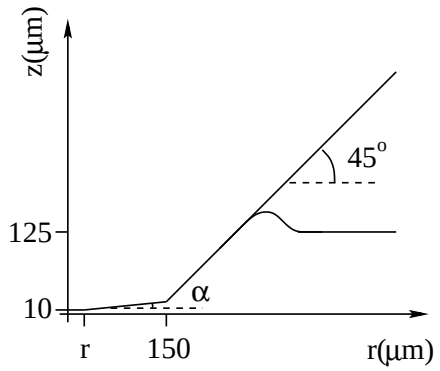

Figure 1: Geometric properties of the model. The central ¤at radius r and the bevel angle α are variable parameters.

Several geometries were considered. Figure 1 describes the main characteristics of the grid used for analyzing the in¤uence of geometric properties of the diamond in the very high pressure experiments. We assumed a gasket preindented to a thickness of 20 μm at the tip from 250 μm at start. The diameter of the diamond bevel is £xed to 300 μm. We have two variable parameters,

Table 1: Central ¤at diameter d and bevel angle α con£gurations.

d (μm)	α (degrees)	d (μm)	α (degrees)
5	8.5°	20	5°
10	8.5°	20	7°
20	8.5°	20	8.5°
50	8.5°	20	10°
		20	12°

*Current address: Laboratoire des Sciences de ta Terre, École Normale Supérieure de Lyon, 46 allée d'Italie, 69364 Lyon Cedex 07, France

†Current address: Geochemistry Department, Sandia National Laboratories, P.O. Box 5800, Albuquerque, NM 87185, U.S.A.

Table 2: *Ab initio* calculated elastic properties of diamond. G_r and G_v are the shear modulus calculated with Reuss and Voigt bounds.

a (Å)	P (GPa)	K (GPa)	C_{44} (GPa)	C_{11} (GPa)	C_{12} (GPa)	G_v (GPa)	G_r (GPa)
3.542	0	459	601	1090	144	550	542
3.535	3	470	601	1101	155	550	542
3.493	21	533	648	1191	204	586	576
3.440	48	622	737	1311	277	649	630
3.281	159	971	915	1767	573	788	754
3.122	339	1482	1163	2389	1028	970	906
2.910	755	2541	1523	3571	2026	1223	1097

the bevel angle α and central ¤at diameter d. Table 1 presents the different con£gurations we examined. We also designed a grid with non-indented gasket in which geometric properties are the same as above except that the gasket thickness is assumed to be 250 μm everywhere.

We considered the diamond as purely elastic with a linear pressure dependence of the elastic constants. These quantities have been measured experimentally[8] and *ab-initio* local density approximation calculations have been previously performed[9, 10], but over a lower range of pressure than considered here. Therefore, we performed new *ab-initio* calculations to higher pressures. Our calculations were carried out using density-functional techniques within the local density approximation (LDA) to electron exchange and correlation. We used a preconditioned conjugate-gradient method to minimize the electronic degrees of freedom. The electronic wave functions were expanded in a plane-wave basis set with periodic boundary conditions. We used norm-conserving and hardness conserving (ENHC) pseudopotentials[11]. This scheme ensures that the total energies of the atom and pseudoatom match to second order with respect to arbitrary changes in valence-state occupancy. This additional condition has been shown to improve pseudopotential transferability in studies of diamond-carbon[11]. The elastic constants were determined using the £nite-deformation method[12, 13, 14, 15]. Table 2 presents the cell parameter, elastic constants and bulk and shear moduli we obtained for different pressures ranging from 0 to 750 GPa. In the £nite-element calculations, we were interested in the 0 to 400 GPa pressure range, so we used the linear approximation of the elastic constants presented in Figure 2.

For the gasket we used a plastic-elastic model with material properties appropriate to rhenium. We assume a shear modulus, a pressure-dependent bulk modulus, and a pressure-dependent yield stress. The bulk modulus and its pressure derivative have been measured experimentally[16, 17]. We used the shear modulus measured from ultrasonic methods[16] at zero pressure. The results presented here are stable towards a variation of this parameter, the most in¤uential property being the yield stress. Experimental studies of the yield stress and its variation with pressure have also been performed [17, 18] but the results have rather large uncertainties (Fig. 3). To have a better constraint on our yield stress estimation, we performed indentation simulations, starting with a non-indented gasket and increasing the load at top surface of the diamond to reach a maximum pressure of about 300 GPa with several models for the gasket yield stress. Following Ref.[17], we used $\sigma_y = 8$ GPa at $P = 0$. Figure 4 presents the shape of the diamond/gasket interface and the corresponding axial stress repartition we obtained. Experimentally, the gaskets compress to a thickness between 5 and 10 μm under multimegabar pressures. Comparing the results in Figure 4(b) we deduce that the gasket model with $\sigma_y = 8$ GPa at 0 GPa and

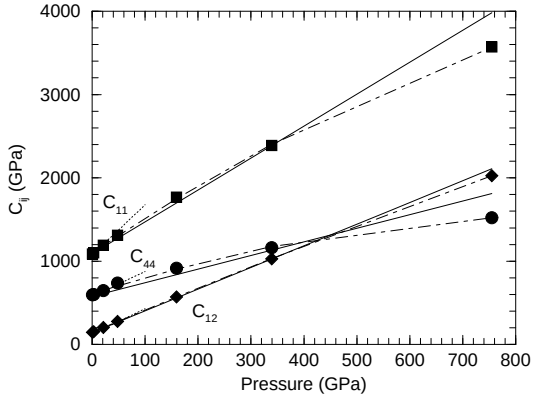

Figure 2: Elastic constants of diamond and their variation with pressure. Square, diamond and circle symbols are C_{11}, C_{12}, and C_{44}, respectively, calculated using *ab-initio* local density approximation. The dotted curves show an extrapolation of ultrasonic experimental measurements[8], dash-dotted curves are polynomial £t through the *ab-initio* data, and solid curves the linear approximation we used in these calculations.

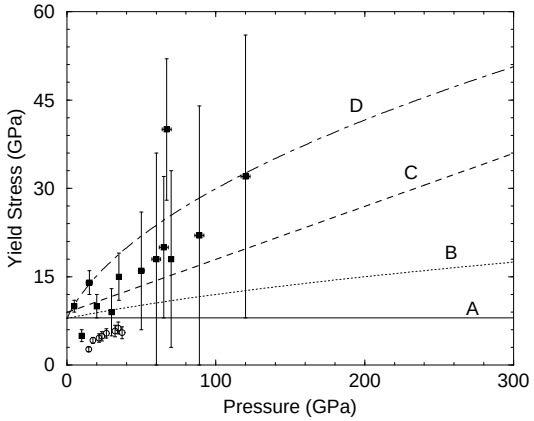

Figure 3: Yield stress of the gasket vs. pressure. The solid and open symbols show data from Ref.[17] and Ref.[18], respectively. Curve A includes no pressure dependence, curves B, C and D present several estimations that satisfy the experimental data.

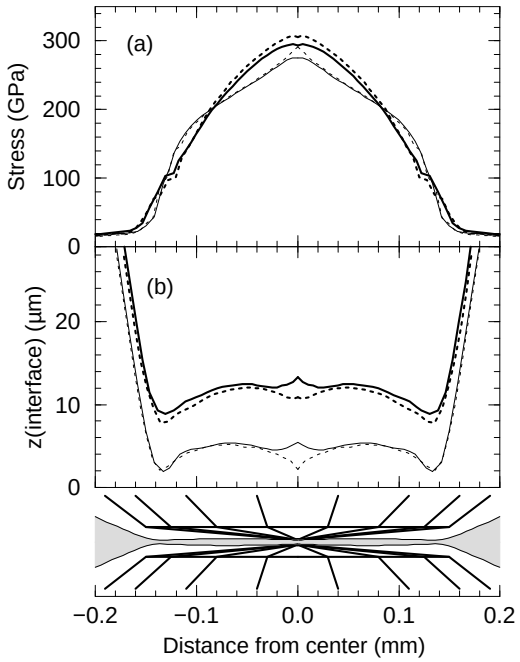

Figure 4: (a), Final calculated axial stress along the diamond/gasket interface, and (b), £nal position of the interface (which gives half the gasket thickness). The thin and solid curves correspond to a gasket yield stress following curve B and D in Figure 3, respectively. The dotted and solid lines are for a 10 and a 50 μm central ¤at diameter diamond, respectively. Deformation of the anvil is shown at the bottom.

12 GPa at 100 GPa (curve B in Figure 3) gives best agreement. This estimation is not unique but gives the right order of magnitude of deformations. The differing behavior between a 10 and 50 μm central ¤at diameter diamond in Figure 4(b) can be explained by the size of the elements used in these calculations, *i.e.* 5 μm.

3. Results

Our material properties being properly constrained, we investigated the in¤uence of the anvil geometry with our preindented gasket models (Fig 1). Figure 5(a,b) present the thickness of the gasket under the diamond tip *versus* pressure at the center of the gasket P_s for the different diamond con£gurations in Table 1. An increase in the bevel angle or a decrease in the central ¤at diameter results in a thinner gasket at megabar pressures. We can distinguish between two different phases on increasing load. The £rst phase involves a compression of the gasket with plastic ¤ow

Table 3: Pressure of transition P_t (in GPa) between the plastic ¤ow and elastic deformations phases and gasket stable thickness h_s (in μm) for different bevel angle α and central ¤at diameter con£gurations d.

d (μm)	α	P_t	h_s	d (μm)	α	P_t	h_s
5	8.5°	245	6.0	20	5°	165	17.2
10	8.5°	240	6.8.	20	7°	215	11.8
20	8.5°	240	8.2	20	8.5°	240	8.2
50	8.5°	230	11.8	20	10°	280	5.6
				20	12°	330	3.6

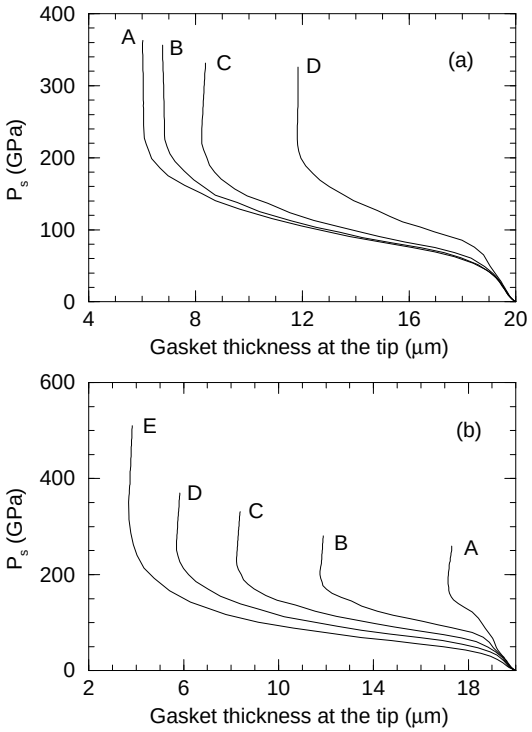

Figure 5: Pressure at the center of the gasket vs. gasket thickness at the tip for different bevel angle α and central ¤at diameter d con£gurations. (a) curves A, B, C, D, $\alpha = 8.5°$ and $d = 5$, 10, 20 and 50 μm respectively. (b) curves A, B, C, D, E, $d = 20$ μm and $\alpha = 5$, 7, 8.5, 10 and 12° respectively.

of material from below the diamond tip towards the edges of the bevel. During the second phase, the gasket thickness at the tip is not modi£ed (vertical lines in Figure 5), the load increase is absorbed by the elastic deformation of the diamond anvil. We can de£ne a transition pressure P_t between the two phases. Its numerical value depends on the geometric properties of the diamond with an increase in the bevel angle or a decrease in the central ¤at diameter tending to increase P_t. Table 3 summarizes the values of P_t and the gasket thickness at the diamond tip during the diamond deformation phase h_s for different central ¤at diameter d and bevel angle α. We observe a saturation when decreasing the central diameter (Fig. 5(a)). Diamond can not be considered as a rigid body under this range of pressures and it tends to accommodate its geometry to the stresses at the tip, thus smoothing the dependence towards the central ¤at diameter.

Figure 6 presents the shape of the diamond/gasket interface and the axial stress repartition for a 10 μm central ¤at diameter and 8.5° bevel angle diamond under different loads of equal increment. As in Figure 5, we observe the two different phases, compression of the gasket with plastic ¤ow of material towards the edges, and elastic deformation of the diamond. As observed in x-ray diffraction experiments[3] we obtain a very clear cupping of the diamond. At the highest loads, the thickness of the gasket at the edge of the bevel is very small and limits the possibility of further deformation of the diamond, leading to a saturation in the pressure vs. load relation.

The axial stress repartition along the diamond/gasket interface is presented on Figure 7 for different diamond geometries under the same load. The bevel angle has a much greater in¤uence than

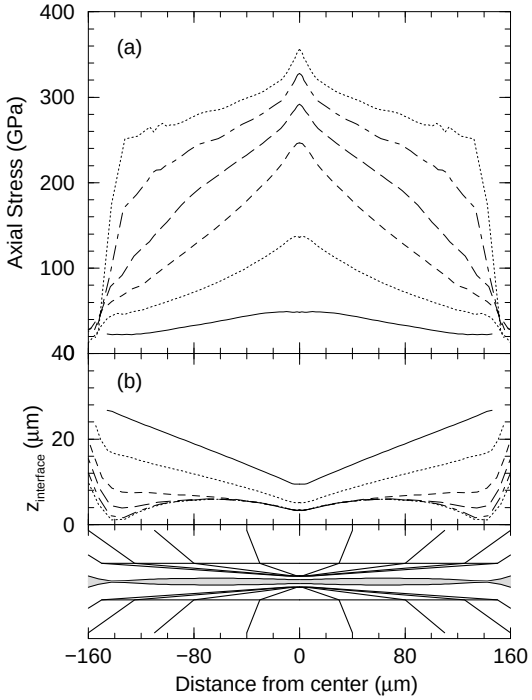

Figure 6: (a) and (b) Calculated axial stress along the diamond/gasket interface and position of this interface (which gives half of the gasket thickness) under different load for a bevel angle of 8.5° and a central ¤at diameter of 10 μm under different loads of equal increment.

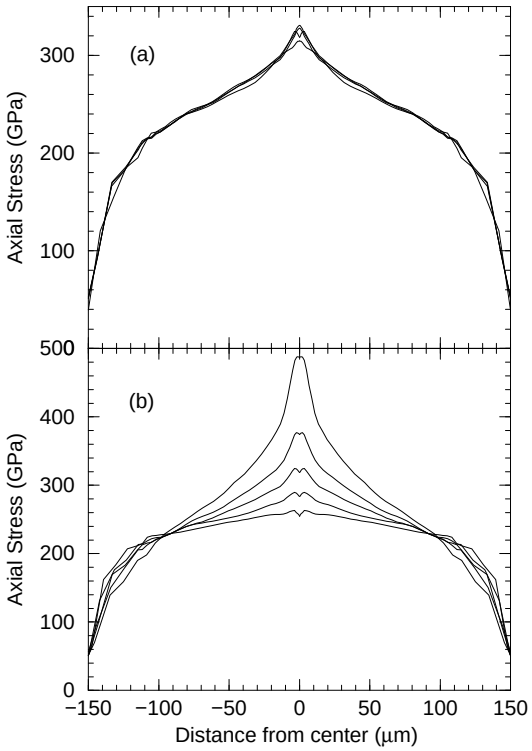

Figure 7: Calculated axial stress along the diamond/gasket interface for different bevel angle α and central ¤at diameter d con£gurations under the same load. (a) $\alpha = 8.5^\circ$ and $d = 5$, 10, 20 and 50 μm, the smallest central ¤at radius gives the highest pressure at the tip. (b) $d = 20$ μm and $\alpha = 5$, 7, 8.5, 10 and 12°, the largest bevel angle gives the highest pressure at the tip.

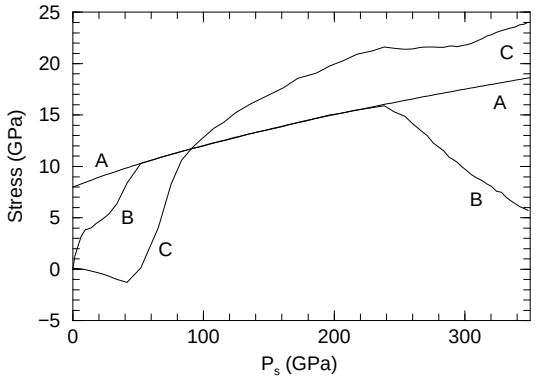

Figure 8: Shear stress at the center of the gasket with an 8.5° bevel angle and 20 μm central ¤at radius diamond. Curve A represents the gasket yield stress σ_y *vs.* pressure, curve B, $2 * \tau$ deduced from the calculation, and curve C is estimated from $2 * \tau \approx -h\ \partial P/\partial r$

the central ¤at diameter because of the saturation phenomenon described above. Increasing the bevel angle or decreasing the central ¤at diameter tends to concentrate the stress at the center of the gasket, resulting in a greater pressure but also larger pressure gradients. Under a pressure at the center of the gasket P_s of about 250 GPa, the pressure gradients at the center of the gasket are -1.42, -1.27, -0.65 and -0.12 GPa/μm for an 8.5° bevel angle and a central ¤at diameter of 5, 10, 20 and 50 μm, respectively; and 0.35, 0.01, -0.65, -2.23 and -4.53 GPa/μm for a 20 μm central ¤at diameter and 5, 7, 8.5, 10 and 12° bevel angle, respectively.

Experimental determination of the exact stress conditions can be dif£cult. Finite-element modeling provides direct access to these quantities at any node of the calculation during simulation of the experiment. For instance we can investigate the state of shear stress τ at the center of the gasket. Previous experiments[17, 19] evaluated this quantity using the relation

$$\tau = \frac{\sigma_{zz} - \sigma_{rr}}{2} \approx -(h/2)\left(\frac{\partial P}{\partial r}\right) \qquad (1)$$

Moreover the yield stress condition gives us the following relation

$$\tau \leq \sigma_y/2 \qquad (2)$$

Figure 8 presents the maximum permitted shear stress $\sigma_y/2$, τ calculated at the center of the gasket, and using equation 1, as a function of pressure for a model with a 20 μm central ¤at diameter and 8.5° bevel angle diamond. We observe three different sections in this £gure; at very low pressures, the system is in a transition mode where it adjusts to the boundary conditions, then it enters the gasket compression mode with plastic ¤ow of material below the diamond tip towards the edges of the bevel. The shear stress τ is at its maximum value (*i.e.* $\sigma_y/2$). At 240 GPa, the transition pressure de£ned in Table 3, the system enters the diamond elastic deformation mode. The gasket shear stress at the tip drops below its maximum value and decreases linearly. There is no longer gasket ¤ow at the tip. Equation 1 is only accurate to within an order of magnitude but has a precision of about 50% in the gasket compression mode and becomes inexact after the transition pressure.

Figure 9 presents the contours of shear stress in a 8.5° bevel angle and 20 μm central ¤at diameter diamond at a sample pressure

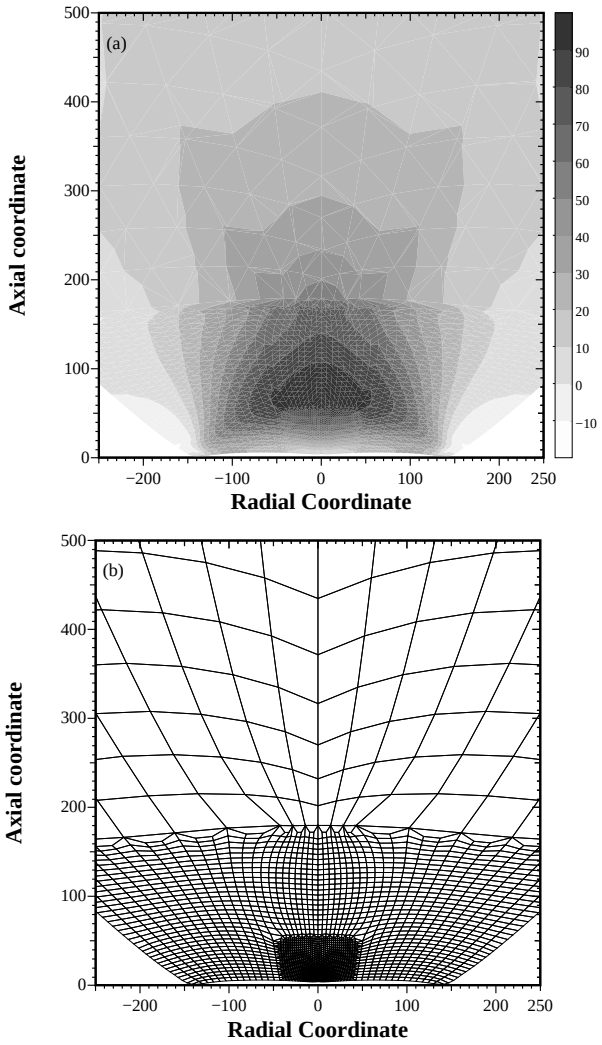

Figure 9: (a) Contours of shear stress $\tau = (\sigma_{zz} - \sigma_{rr})/2$ for an 8.5° bevel angle and 20 μm central ¤at radius diamond, with a sample pressure of 350 GPa. The coordinates are in μm and the stresses in GPa. The discontinuities were generated because of transitions in the £nite-element mesh. (b) The deformed £nite-element mesh under these conditions.

Table 4: Relation between the maximum shear stress in the diamond τ_{MAX} after the transition pressure P_t and the pressure at the center of symmetry P_s, and pressure of failure P_f according to relation 4 for different central ¤at diameter d and bevel angle α con£gurations.

d(μm)	α	τ_{MAX} (GPa)	P_f (GPa)
5	8.5°	$-24 + 0.355\ P_s$	349
10	8.5°	$-25 + 0.360\ P_s$	345
20	8.5°	$-23 + 0.353\ P_s$	348
50	8.5°	$-23 + 0.364\ P_s$	338
20	5°	$-14 + 0.376\ P_s$	303
20	7°	$-23 + 0.381\ P_s$	323
20	8.5°	$-23 + 0.353\ P_s$	348
20	10°	$-25 + 0.326\ P_s$	383
20	12°	$-7 + 0.241\ P_s$	444

of about 350 GPa. The point of maximum shear stress τ_{MAX} is located close to the symmetry axis, about 60 μm above the tip. In this particular case

$$\tau_{MAX} \approx 100 \text{ GPa} \tag{3}$$

Recent *ab-initio* calculation[20] predicted a mechanical instability of diamond when

$$\sigma_{zz} - \sigma_{rr} = 200 \text{ GPa} \tag{4}$$

This condition is reached in this £gure. In general, this range of shear stress can only be reached in the second phase of the loading, when the diamonds are elastically deforming. After the transition pressure, the maximum shear stress in the diamond and the pressure at the center of the gasket are linearly related. The coef£cients of the £t are presented in Table 4. We can estimate a pressure of failure P_f when condition given by Equation 4 is reached for each geometry (Table 4). According to this model, an increase in bevel angle diminishes the maximum shear stress, allowing the attainment of greater sample pressures before diamond failure. The use of large bevel angles has been limited experimentally because of diamond failure at very low pressures, before any diamond elastic deformation. This weakness is probably not related to high shear stress in the diamond. Figure 5 shows that a large bevel angle results in greater gasket ¤ow below the diamond tip during the compression phase. This might lead to instabilities in the case of defects or weaknesses in the gasket.

Finally, Table 5 presents the calculated stress conditions at three different locations in the diamond for different pressures in the gasket, on the symmetry axis near the tip, near the maximum shear stress, and in the high shear stress zone (but away from the tip). These numbers are critical for understanding the changes in optical properties of diamond anvils, and analyzing the band-gap behavior of the anvils in diamond cells as a function of the sample pressure or load.

4. Conclusions

A £nite-element analysis shows that plastic and elastic models are suf£cient to simulate the behavior of the anvils in the diamond cell at multimegabar pressures. The elastic properties of diamond were calculated using *ab initio* local density approximation methods over a very large range of static pressures. We also obtained an estimate of the dependence of the gasket yield stress on pressure As show previously[4], the model reproduces the very large elastic deformation of the diamond, leading to a clear cupping of the anvils. The pressure increase can be separated into two different phases: initial compression of the gasket with plastic ¤ow of material from the tip towards the edges of the bevel, coupled with subsequent elastic deformation of the anvils. The pressure of transition between these two phases depends on the geometry of the anvils.

Investigation of the exact stress conditions showed that the shear stress at the center of the gasket is at a maximum during the £rst phase of the pressure increase and drops drastically during the diamond deformation phase. The maximum shear stress in the diamond is found to decrease with the bevel angle. The high value shear stress in the anvil could lead to mechanical instability for sample pressures as low as 300 GPa.

Table 5: Stress history at selected locations in the diamond. Location A is on the z-axis and $z \approx 2$ μm, location B is on the z-axis and $z \approx 65$ μm, where the shear stress is maximum, and location C, is at $r \approx 70$ μm and $z \approx 60$ μm, the z coordinates being reported to the tip position. P_s is the pressure at the center of the gasket and P the pressure at the location.

Position	P_s (GPa)	σ_{rr} (GPa)	$\sigma_{\theta\theta}$ (GPa)	σ_{zz} (GPa)	σ_{rz} (GPa)	P (GPa)
A	9	5.5830e+00	5.5680e+00	1.1360e+01	1.4790e-02	7.5037e+00
A	52	3.2710e+01	3.2740e+01	6.0210e+01	8.3510e-01	4.1887e+01
A	100	5.6600e+01	5.6320e+01	1.0360e+02	2.1750e+00	7.2173e+01
A	150	9.1450e+01	9.0770e+01	1.5270e+02	3.3240e+00	1.1164e+02
A	197	1.2530e+02	1.2420e+02	1.9920e+02	4.5740e+00	1.4957e+02
A	254	1.7580e+02	1.7400e+02	2.5400e+02	5.3800e+00	2.0127e+02
A	302	2.3200e+02	2.2960e+02	2.9580e+02	5.4590e+00	2.5247e+02
A	349	2.9190e+02	2.8900e+02	3.3830e+02	5.8090e+00	3.0640e+02
B	9	2.3080e+00	2.3100e+00	9.9910e+00	7.4630e-02	4.8697e+00
B	52	6.5680e+00	6.5820e+00	3.6820e+01	4.0360e-01	1.6657e+01
B	100	1.0800e+01	1.0820e+01	5.9080e+01	6.4310e-01	2.6900e+01
B	150	1.4830e+01	1.4870e+01	8.4850e+01	9.7700e-01	3.8183e+01
B	197	1.7540e+01	1.7590e+01	1.0770e+02	1.3250e+00	4.7610e+01
B	254	2.1930e+01	2.2000e+01	1.4540e+02	1.7690e+00	6.3110e+01
B	302	2.9180e+01	2.9300e+01	1.9270e+02	2.0080e+00	8.3727e+01
B	349	4.0360e+01	4.0530e+01	2.4000e+02	1.9910e+00	1.0696e+02
C	9	2.6510e+00	2.9010e+00	1.0160e+01	1.5660e+00	5.2373e+00
C	52	8.7620e+00	8.7180e+00	3.0780e+01	7.1460e+00	1.6087e+01
C	100	1.4600e+01	1.4590e+01	4.8800e+01	1.0970e+01	2.5997e+01
C	150	2.1160e+01	2.0720e+01	6.8450e+01	1.6090e+01	3.6777e+01
C	197	2.6430e+01	2.5360e+01	8.5320e+01	2.1110e+01	4.5703e+01
C	254	3.4730e+01	3.3170e+01	1.1560e+02	3.0280e+01	6.1167e+01
C	302	4.4360e+01	4.6110e+01	1.6550e+02	4.0600e+01	8.5323e+01
C	349	5.7130e+01	6.6470e+01	2.2590e+02	4.5180e+01	1.1650e+02

References

[1] H. K. Mao and P. M. Bell, Science **200**, 1145 (1978).

[2] P. M. Bell, H. K. Mao, and K. Goettel, Science **226**, 542 (1984).

[3] R. J. Hemley, H. K. Mao, G. Shen, J. Badro, P. Gillet, M. Han¤and, and D. Häusermann, Science **276**, 1242 (1997).

[4] S. Merkel, R. J. Hemley, and H. K. Mao, Appl. Phys. Lett. **74**, 656 (1999).

[5] M. S. Bruno and K. J. Dunn, Rev. Sci. Instrum. **55**, 940 (1984).

[6] W. C. Moss, J. O. Hallquist, R. Reichlin, K. A. Goettel, and S. Martin, Appl. Phys. Lett. **48**, 1258 (1986).

[7] W. C. Moss and K. A. Goettel, Appl. Phys. Lett. **50**, 25 (1987).

[8] H. J. McSkimin and P. Andreatch Jr., J. Appl. Phys. **43**, 2944 (1972).

[9] O. H. Nielsen, Phys. Rev. B **34**, 5808 (1986).

[10] O. H. Nielsen and R. M. Martin, Phys. Rev. B **32**, 3780 (1985).

[11] M. P. Teter, Phys. Rev. B **48**, 5031 (1993).

[12] M. J. Mehl, J. E. Osburn, D. A. Papaconstantopoulos, and B. M. Klein, Phys. Rev. B **41**, 10311 (1990).

[13] M. J. Mehl, Phys. Rev. B **47**, 2493 (1993).

[14] M. J. Mehl, D. J. Singh, and D. A. Papaconstantopoulos, Material Science and Engineering **A170**, 49 (1993).

[15] M. J. Mehl, D. J. Singh, and D. A. Papaconstantopoulos, in *Intermetallic Compounds: Principles and Applications*, edited by J. H. Westbrook and R. L. Fleisher (John Wiley & Sons Ldt, 1994).

[16] M. H. Manghnani and K. Katahara, Phys. Rev. B **9**, 1421 (1974).

[17] R. Jeanloz, B. K. Godwal, and C. Meade, Nature (London) **349**, 687 (1991).

[18] T. S. Duffy, G. Shen, D. L. Heinz, J. Shu, Y. Ma, R. J. Hemley, H. K. Mao, and A. K. Singh, Phys. Rev. B **60**, 1 (1999)

[19] C. Meade and R. Jeanloz, J. Geoph. Res. **93**, 3261 (1988).

[20] J. J. Zhao, S. Scandolo, J. Kohanoff, G. L. Chiarotti, and E. Tosatti, Appl. Phys. Lett. **75**, 487 (1999).